Molecular and Phenotypic Analysis of *Attractin* Mutant Mice

T. M. Gunn,*,[1] T. Inui,[†] K. Kitada,[‡] S. Ito,[§] K. Wakamatsu,[§] L. He,* D. M. Bouley, T. Serikawa[‡] and G. S. Barsh***

**Departments of Pediatrics and Genetics, and the Howard Hughes Medical Institute, Stanford University School of Medicine, Stanford, California 94305, [†]Safety Research Laboratory, Tanabe Seiyaku Co. Ltd., Yodogawa-ku, Osaka 532-8505, Japan, [§]Fujita Health University School of Health Sciences, Toyoake, Aichi 470-1192, Japan, **Department of Comparative Medicine, Stanford University School of Medicine, Stanford, California 94305 and [‡]Institute of Laboratory Animals, Kyoto University, Sakyo-ku, Kyoto 606-8501, Japan*

Manuscript received March 9, 2001
Accepted for publication May 29, 2001

ABSTRACT

Mutations of the mouse *Attractin* (*Atrn*; formerly *mahogany*) gene were originally recognized because they suppress *Agouti* pigment type switching. More recently, effects independent of *Agouti* have been recognized: mice homozygous for the $Atrn^{mg\text{-}3J}$ allele are resistant to diet-induced obesity and also develop abnormal myelination and vacuolation in the central nervous system. To better understand the pathophysiology and relationship of these pleiotropic effects, we further characterized the molecular abnormalities responsible for two additional *Atrn* alleles, $Atrn^{mg}$ and $Atrn^{mg\text{-}L}$, and examined in parallel the phenotypes of homozygous and compound heterozygous animals. We find that the three alleles have similar effects on pigmentation and neurodegeneration, with a relative severity of $Atrn^{mg\text{-}3J} > Atrn^{mg} > Atrn^{mg\text{-}L}$, which also corresponds to the effects of the three alleles on levels of normal *Atrn* mRNA. Animals homozygous for $Atrn^{mg\text{-}3J}$ or $Atrn^{mg}$, but not $Atrn^{mg\text{-}L}$, show reduced body weight, reduced adiposity, and increased locomotor activity, all in the presence of normal food intake. These results confirm that the mechanism responsible for the neuropathological alteration is a loss—rather than gain—of function, indicate that abnormal body weight in *Atrn* mutant mice is caused by a central process leading to increased energy expenditure, and demonstrate that pigmentation is more sensitive to levels of *Atrn* mRNA than are nonpigmentary phenotypes.

THE mouse *Attractin* (*Atrn*; formerly *mahogany*) gene encodes a single-pass transmembrane protein that is involved in regulating the switch in pigment type synthesis from eumelanin (brown or black) to pheomelanin (yellow or red) via the Mc1r-Agouti signaling pathway (Miller *et al.* 1997; Gunn *et al.* 1999; Nagle *et al.* 1999). The melanocortin 1 receptor (Mc1r) is a G-protein-coupled receptor, expressed on melanocytes, that increases intracellular levels of cyclic adenosine monophosphate (cAMP) either in response to the presence of α-melanocyte stimulating hormone (α-MSH) or to constitutive levels of activity, leading to the production of eumelanin. Agouti protein is a paracrine signaling molecule secreted by cells of the dermal papilla that acts as an endogenous antagonist of Mc1r signaling in melanocytes within the hair follicle. When Agouti protein is present, Mc1r signaling is inhibited and consequently the melanocytes produce pheomelanin instead of eumelanin (reviewed in Jackson 1994). Agouti is normally expressed only during the midportion of the hair growth cycle, resulting in production of brown or black hairs with a subapical band of yellow pigment. In Agouti (*A/-*) mice, loss-of-function mutations in *Atrn* reduce or eliminate synthesis of pheomelanin (Lane and Green 1960; Miller *et al.* 1997), suggesting that *Atrn* is necessary for the antagonistic action of Agouti protein on the Mc1r. We recently showed that Atrn specifically binds Agouti protein *in vitro*, implicating it as a low affinity accessory receptor required for Agouti protein signaling through the Mc1r (He *et al.* 2001).

Loss of Atrn suppresses not only the normal effects of Agouti on pigment production but also the pleiotropic effects of ectopic Agouti expression observed in mice carrying the lethal-yellow (A^y) allele at the Agouti locus (Miller *et al.* 1997; Dinulescu *et al.* 1998; He *et al.* 2001). A^y animals ubiquitously express Agouti protein and as a result produce only yellow pigment, show increased linear growth, and develop juvenile onset obesity and hyperinsulinemia. The metabolic effects of ectopic Agouti expression are thought to arise from its expression in the brain and its ability to antagonize signaling through the Mc4r. Normally, signaling through the Mc4r is activated by α-MSH and antagonized by Agouti-related protein (Agrp), which shares structural similarity to Agouti at its carboxyl terminus (Ollmann *et al.* 1997; Shutter *et al.* 1997; Yang *et al.* 1999). Null mutations in Mc4r and ectopic overexpression of Agrp cause a metabolic phenotype similar to

Corresponding author: Greg Barsh, Beckman Ctr., Stanford University School of Medicine, Stanford, CA 94305-5323.
E-mail: gbarsh@cmgm.stanford.edu

[1] *Present address:* Department of Biomedical Sciences, T4018 VRT, Cornell University, Ithaca, NY 14853. E-mail: tmg25@cornell.edu

that seen in A^y mice (Huszar *et al.* 1997; Ollmann *et al.* 1997) but, interestingly, these forms of obesity are not suppressed by *Atrn* mutations (Nagle *et al.* 1999; He *et al.* 2001). These observations indicate that suppression of A^y-induced obesity is specific to an interaction between Agouti and Atrn and not due to a general role of Atrn in melanocortin signaling pathways. However, homozygosity for $Atrn^{mg\text{-}3J}$ causes reduced body weight in the absence of A^y (He *et al.* 2001) and partially suppresses obesity caused by consumption of a high fat diet (Nagle *et al.* 1999).

Several features suggest a fundamental role for Atrn in central nervous system (CNS) development and/or function. Atrn has many structural characteristics of molecules implicated in cell adhesion or axon guidance, and Atrn RNA is widely expressed throughout the CNS in specific sets of neurons with no obvious underlying anatomic or functional relationship (Lu *et al.* 1999). In a histopathologic survey of $Atrn^{mg\text{-}3J}/Atrn^{mg\text{-}3J}$ mice, we found widespread vacuolation throughout the brain and spinal cord (He *et al.* 2001). In addition, Kuramoto *et al.* (2001) recently discovered that the phenotype of the *zitter* rat, a well-characterized model for spongy degeneration and hypomyelination in the CNS associated with tremor and flaccid paresis (Rehm *et al.* 1982; Kondo *et al.* 1992, 1995), is caused by a loss-of-function mutation in *Atrn*.

Comparative analysis of an allelic series can provide insight into the molecular basis of a pleiotropic phenotype caused by mutation in a single gene. The effects of mutations in *Atrn* on neurodegeneration and body weight (in the absence of A^y), however, have been measured only for $Atrn^{mg\text{-}3J}$ (He *et al.* 2001; Kuramoto *et al.* 2001). There are two additional alleles, $Atrn^{mg}$ and $Atrn^{mg\text{-}L}$, which are caused by ~5-kb intronic insertions and have coat color phenotypes less severe than $Atrn^{mg\text{-}3J}$ (Gunn *et al.* 1999; Nagle *et al.* 1999). Here, we compare the effects of these three alleles on pigmentation, adiposity, food consumption, and neurodegeneration. Our results confirm that the *Atrn* gene by itself plays a significant role in body weight regulation that is independent of Agouti function but likely related to the neurodegeneration observed in *Atrn* mutants. In addition, the level of Atrn required for normal pigment production appears to be higher than that required for normal neuronal function and metabolism as $Atrn^{mg\text{-}L}$ homozygotes demonstrate an obvious pigmentation defect but have normal body weight and little or no vacuolation. Finally, we describe a subtle pigmentation phenotype in *Atrn* mutant mice that is also likely independent of Agouti, which suggests a potential explanation for how the pleiotropic effects of *Atrn* may have been acquired during vertebrate evolution.

MATERIALS AND METHODS

Mice: There are three available mutant alleles at the *Atrn* locus: $Atrn^{mg\text{-}3J}$, $Atrn^{mg}$, and $Atrn^{mg\text{-}L}$. Mice homozygous for the $Atrn^{mg\text{-}3J}$ mutation were originally obtained from the Jackson Laboratory (Bar Harbor, Maine). The $Atrn^{mg\text{-}3J}$ mutation arose in the C3HeB/FeJ strain and has been maintained on the C3H/HeJ background for over 150 generations. Mice homozygous for the $Atrn^{mg\text{-}L}$ mutation were kindly supplied by Jean Westerman at The University of Warwick. This mutation arose in C3H/HeJ in 1981 and has continued to be maintained on that background. The $Atrn^{mg}$ mutation arose in 1950 in a cross between a C3H female and a Swiss stock male (Lane and Green 1960). At closely linked genetic markers, $Atrn^{mg}$ mice segregate C3H alleles, suggesting that the original mutation affected the C3H-derived chromosome. At F_{27}, these C3H-Swiss background $Atrn^{mg}$ mutants were crossed to C57BL/10Gn × CBA/Ca-se F_3 animals carrying the *limb deformity* mutation (*ld*, now $formin^{ld}$) to create the LDJ/Le strain (Festing 1996). These mice were obtained from the Jackson Laboratory and we backcrossed the $Atrn^{mg}$ mutation from this background back onto C3H/HeJ. The animals used in this study had been backcrossed for six generations (N_6F_1-N_6F_4), at which point they are expected to derive over 98% of their genome from C3H/HeJ. C57BL/6J-$A^{w\text{-}J}/A^{w\text{-}J}$ mice were obtained from the Jackson Laboratory. C57BL/6J-a^e/a^e mice, which are phenotypically indistinguishable from C57BL/6J-*mg/mg* mice until 4–5 months of age (see below), were a gift from Linda Siracusa (Department of Microbiology and Immunology, Jefferson Medical College), who backcrossed the a^e mutation from the AEJ strain onto C57BL/6J; the animals used in these experiments were $N_{12}F_1$-$N_{12}F_3$. $Atrn^{gt}/Atrn^{gt}$ mice were a gift from Phil Leighton and Marc Tessier-Lavigne (University of California, San Francisco, School of Medicine). All mice were maintained under standard conditions within the Department of Comparative Medicine at Stanford University and fed standard lab chow.

Physiological assays: For all studies, sex-matched sib pairs of mutant and nonmutant animals were compared. The experiment was designed such that food consumption, activity, and adiposity assays were carried out on the same animals as described below. For longitudinal measurement of body weight, male mice were singly caged while females were housed with up to four female littermates. For measurement of food intake, all mice were housed individually for at least 1 week prior to the experiment. While recording food consumption, the mice were weighed before the experiment and then given a minimal amount of nonedible bedding, such that small pieces of food (weighing as little as 0.1 g) could easily be found. Each afternoon, four to five fresh pellets of food were weighed and then placed on the cage floor. The pellets and any visible small fragments were removed every 24 hr, weighed, and discarded; any animals with pellet fragments so small as to prevent collection were removed from the sample. Average daily food consumption per animal was calculated from measurements taken over at least 5 consecutive days.

After 5–7 days of measuring food intake, home cage locomotor activity was assessed on each mouse using a photobeam cage system (San Diego Instruments, CA), as described by Hein *et al.* (1995). One pair of mutant and nonmutant sibs was examined at a time and care was taken to alternate the frame into which the mutant animal was placed. The animals had generally been weighed monthly since weaning and their food consumption was recorded as above, but they had not been used for any other experiments. Animals were placed into the experimental cage at least 17 hr prior to the start of activity recording. Data were recorded for 48 hr, starting between noon and 5 p.m. Each cage contained one mouse, a sparse amount of bedding, and ample food pellets spread evenly across the bottom of the cage. Water bottles were hung from the side of the cage, which was enclosed by a plastic microisolator unit (no wire lid for the animals to hang on).

Following activity recording, the animals were weighed, and then total lipid content was determined by saponifying the animals in alcoholic potassium hydroxide and measuring glycerol content of neutralized samples enzymatically, using the triglyceride GPO trinder assay (Sigma, St. Louis; Lowell *et al.* 1993; Shimada *et al.* 1998).

Chemical analysis of hair melanins: Hairs were plucked from the middorsum of two animals per genotype. For the HPLC determination of eumelanin, hair samples were oxidized with permanganate to give pyrrole-2,3,5-tricarboxylic acid (PTCA), with ultraviolet detection (Ito and Fujita 1985; Ozeki *et al.* 1995). For the HPLC determination of pheomelanin, hair samples were hydrolyzed with hydriodic acid to give aminohydroxyphenylalanine (AHP), which was quantified with electrochemical detection (Ito and Fujita 1985). One nanogram of PTCA corresponds to ~50 ng of eumelanin and 1 ng of AHP corresponds to ~5 ng of pheomelanin (Ito and Fujita 1985; Ito and Wakamatsu 1998).

Molecular biology: Southern hybridization of genomic DNA prepared from normal and mutant (*Atrn*^{mg} and *Atrn*$^{mg\text{-}L}$) animals with cDNA and genomic DNA probes revealed restriction fragment length polymorphisms between the parental C3H/HeJ strain and mutant animals, and long-range PCR (Expand Long Template polymerase, Roche, CA) across these regions demonstrated an ~5-kb insertion (Gunn *et al.* 1999). These PCR products were cloned into pCRII-TOPO and pCR-XL-TOPO (Invitrogen, San Diego) and ~1 kb of sequence was generated, from both strands, for either end of the insertion. Sequences were compared to consensus intracisternal A particle (IAP) sequence X04120 in GenBank. The *Atrn*$^{mg\text{-}3J}$ mutation was first reported by Nagle *et al.* (1999) as a 5-bp deletion within the *Atrn* cDNA sequence. Because the deletion lies near the 3′ end of an exon, long-range PCR was used to amplify across the intervening intron to allow sequencing of both strands to confirm the position and nature of the mutation. Polyadenylated RNA was isolated from adult whole brain tissue using the Oligotex direct mRNA maxi kit (QIAGEN, Valencia, CA). The *Atrn* cDNA probes used for Northern hybridization were as follows: 5′TM is a 461-bp cDNA fragment that ends 401 bp upstream of the beginning of the transmembrane domain-encoding region; 3′ TM is a 463-bp cDNA fragment that overlaps the transmembrane domain-encoding region by 9 bp and continues downstream; 3′ untranslated region (UTR) is the ~700-bp insert of IMAGE clone 722527, which contains sequence from the most 3′ region of the *Atrn* 3′ UTR. A *Gapd* probe was used to estimate RNA loading. Production and characterization of Atrn antibodies will be described in detail elsewhere; in brief, a polyclonal antisera raised against a glutathione *S*-transferase fusion protein containing amino acids 666–782 of mouse Atrn was affinity purified and then used for Western blot analysis of brain extracts as previously described (Gunn *et al.* 1999). Whole brain was homogenized in radioimmuno precipitation (RIPA) buffer, and proteins were separated by 4–20% SDS-PAGE under reducing conditions before transfer to a nylon membrane. After incubation with primary antiserum at 1:1000 dilution, immobilized Atrn protein was detected with goat anti-rabbit IgG and a chemiluminescence system.

Histopathology: Brains and spinal cords were collected from *Atrn* mutant and nonmutant animals at 1, 2, 4, or 8 months of age, fixed, sectioned, stained, and examined by light microscopy as previously described (Inui *et al.* 1990; He *et al.* 2001; Kuramoto *et al.* 2001).

Statistical analysis: Average hair melanin content, body weight, body fat, food consumption, and activity levels of mutant and nonmutant animals were analyzed for significant differences by a two-sample *t*-test. For food consumption and body fat determinations, effects due to differences in the age of animals were accounted for by calculating the values for mutant animals as a percentage of that of their nonmutant age- and sex-matched littermates. No corrections were made for multiple testing.

RESULTS

Coat color phenotype of three Atrn mutants: There are three previously existing *Attractin* mutant alleles: *Atrn*^{mg}, *Atrn*$^{mg\text{-}3J}$, and *Atrn*$^{mg\text{-}L}$. In addition, Leighton *et al.* (2001) recently described a new allele that arose out of a gene trap screen and is referred to below as *Atrn*^{gt}. C3H/HeJ animals carry the *A* allele at the *Agouti* locus and normally have banded (black-yellow-black) hairs. On a C3H/HeJ background, the *Atrn*$^{mg\text{-}3J}$ mutation has the strongest pigmentation phenotype, with no visible yellow pigment in coat hairs of homozygous animals. Next strongest is the *Atrn*^{mg} mutation, which produces homozygous animals with dark backs but some yellow pigment in their flank and ventral hairs. Mice homozygous for the *Atrn*$^{mg\text{-}L}$ mutation have the weakest phenotype: They appear similar to *Atrn*^{mg} homozygotes but with a narrower dorsal "stripe" of black and more visible yellow pigment (Gunn *et al.* 1999). The *Atrn*^{gt} allele has not been examined on a C3H background; however, homozygotes on a mixed 129-C57BL/6J background are intermediate in phenotype between *Atrn*^{mg} and *Atrn*$^{mg\text{-}3J}$ homozygotes. As might be expected for an additive interaction, *Atrn*$^{mg\text{-}3J}$/*Atrn*^{mg} compound heterozygotes are darker than *Atrn*$^{mg\text{-}3J}$/*Atrn*$^{mg\text{-}L}$, which are in turn darker than *Atrn*^{mg}/*Atrn*$^{mg\text{-}L}$ (data not shown).

As a more quantitative measure of *Atrn* gene action, we determined the amount of pheomelanin and eumelanin in hairs from mutant mice. Chemical hydrolysis or oxidation of biologic samples yields two derivatives, AHP and PTCA, respectively, that can be used to estimate the amounts of pheomelanin and eumelanin that were originally present (Ito and Fujita 1985). Comparing AHP content among dorsal hairs plucked from 4- to 7-week-old mice, we found that all homozygous and compound heterozygous *Atrn* mutants showed an AHP content 5- to 10-fold lower than nonmutant C3H/HeJ animals ($P < 0.001$), with differences in AHP content among mutant animals roughly proportionate to what is observed visually (Figure 1A). Thus, hairs from *Atrn*$^{mg\text{-}3J}$ homozygotes contained less AHP than *Atrn*^{mg} and *Atrn*$^{mg\text{-}L}$ homozygotes, whereas hairs from compound heterozygotes contained intermediate levels. No difference in AHP content was detected between hairs from *Atrn*^{mg} and *Atrn*$^{mg\text{-}L}$ homozygotes even though *Atrn*$^{mg\text{-}L}$ mutant animals are visibly lighter than *Atrn*^{mg} mutant animals (Gunn *et al.* 1999). Levels of AHP in hairs from compound heterozygotes were intermediate between the values for parental homozygotes (Figure 1A), confirming the impression that the alleles interact in an additive manner.

In 5- to 7-week-old mice, levels of eumelanin-derived

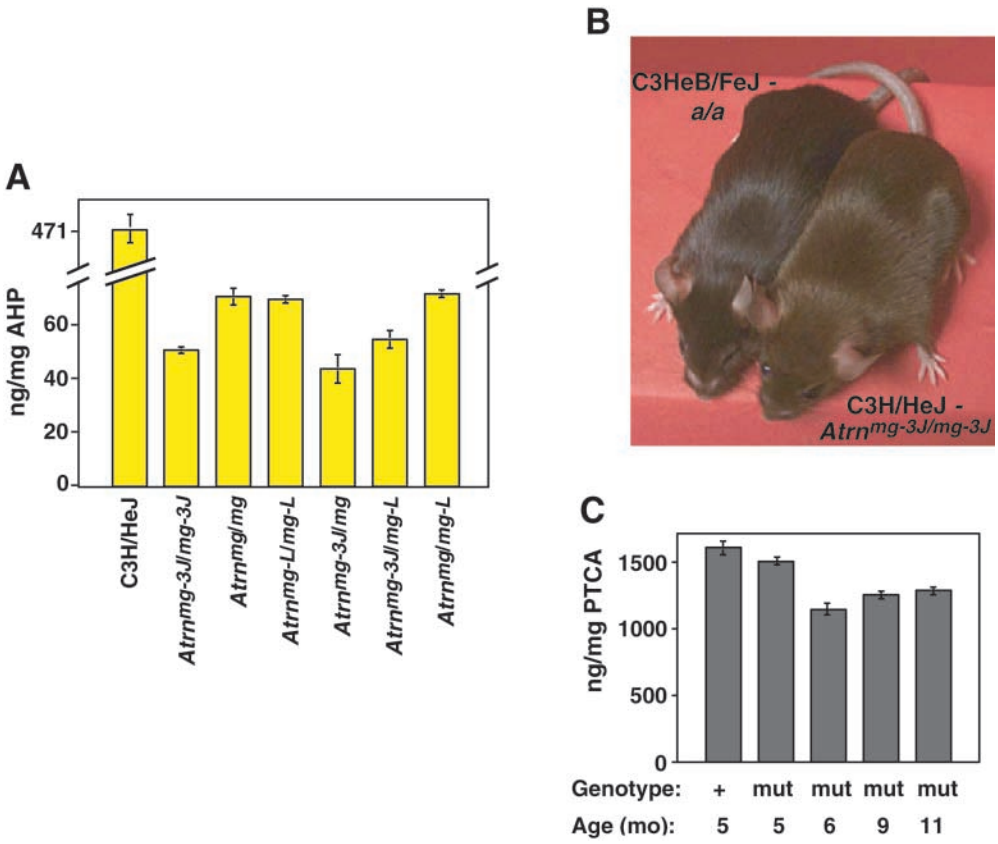

FIGURE 1.—Coat color phenotype associated with mutant *Atrn* alleles. (A) Average AHP content in dorsal hairs from 4- to 7-week-old *Atrn* mutants compared to C3H/HeJ animals. Values are given as nanograms of AHP per milligram of hair. Mice homozygous for each of the mutant *Atrn* alleles ($Atrn^{mg\text{-}3J}$, $Atrn^{mg}$, and $Atrn^{mg\text{-}L}$) as well as compound heterozygotes have significantly decreased levels of pheomelanin ($P < 0.001$). (B) Older *Atrn* mutant animals, as seen by comparing 6-month-old C3H/HeJ-$Atrn^{mg\text{-}3J}/Atrn^{mg\text{-}3J}$ and C3HeB/FeJ-*a/a* animals; the $Atrn^{mg\text{-}3J}A/Atrn^{mg\text{-}3J}$ *A* mutant is dark reddish brown whereas the + *a*/+ *a* animal is completely black. (C) Average PTCA content in dorsal hairs from 5- to 12-month-old $Atrn^{mg\text{-}3J}$ mutants. Values are given as nanograms of PTCA per milligram of hair.

PTCA in hairs of *Atrn* mutant mice were slightly reduced compared to C3H/HeJ animals (not shown). However, during the course of this work, we noted that *Atrn* mutant animals acquire a dark reddish brown appearance as they age. This change in coloration, reminiscent of the wood for which the mutation was named originally, affects the entire hair shaft, is more obvious in $Atrn^{mg\text{-}3J}$ than in the other two alleles, but is subtle and most apparent in a direct comparison of mutant to nonmutant animals (Figure 1B). We measured eumelanin-derived PTCA levels in older $Atrn^{mg\text{-}3J}$ mutant animals and observed a 20–30% reduction between 5 and 11 months of age (Figure 1C). Taken together, these observations suggest that Atrn has effects on pigmentation that are independent of *Agouti*-induced pigment type-switching.

Molecular identity/characterization of mutant *Atrn* alleles: The severity of the pigmentation defect in mice carrying different *Atrn* alleles is consistent with the changes observed at the molecular level. Using Northern hybridization to total RNA, $Atrn^{mg\text{-}3J}$ mutant animals make no detectable transcript, while the $Atrn^{mg}$ and $Atrn^{mg\text{-}L}$ mutants make a small amount of normal-sized transcript as well as more abundant aberrant isoforms (GUNN *et al.* 1999). NAGLE *et al.* (1999) found that the mutation in $Atrn^{mg\text{-}3J}$ mice is a 5-bp deletion near the end of exon 16 that results in a frameshift mutation such that the first 914 codons are unchanged but codon 915 is changed from a serine to a leucine and a premature stop codon is introduced at position 916 (Figure 2A). This mutation presumably results in instability of the transcript due to nonsense-mediated decay, although small amounts of mRNA are detectable by Northern hybridization to polyadenylated RNA (Figure 2B).

To better understand the molecular basis of the phenotypic differences between $Atrn^{mg\text{-}3J}$, $Atrn^{mg}$, and $Atrn^{mg\text{-}L}$ mutants, we isolated and partially sequenced the ~5-kb insertions in $Atrn^{mg}$ and $Atrn^{mg\text{-}L}$ (GUNN *et al.* 1999), which lie in adjacent introns, downstream of the exons encoding the transmembrane domain. In each case, we found insertion of an IAP element with 5′- and 3′-end sequences matching GenBank X04120. In $Atrn^{mg\text{-}L}$ animals the IAP element is inserted in intron 27 in a 5′ to 3′ orientation, while the IAP element in $Atrn^{mg}$ animals is inserted in intron 26, in the reverse orientation (Figure 2A). On the basis of Northern hybridization results (GUNN *et al.* 1999 and Figure 2B), both insertions appear to affect normal splicing. In $Atrn^{mg\text{-}L}$ mutants, some normal-sized transcript is made as well as a smear of larger mRNA isoforms; the larger mRNAs likely terminate within the IAP as they are detected only by cDNA probes (5′ TM and 3′ TM, Figure 2A) that contain sequences upstream of the $Atrn^{mg\text{-}L}$ insertion site (Figure 2B and data not shown). In $Atrn^{mg}$ mutants, a faint normal-sized transcript apparent in total RNA is not apparent in polyadenylated RNA (Figure 2B), but the larger transcript observed in total RNA (GUNN *et al.*, 1999) is also detected in polyadenylated RNA, with probes from any

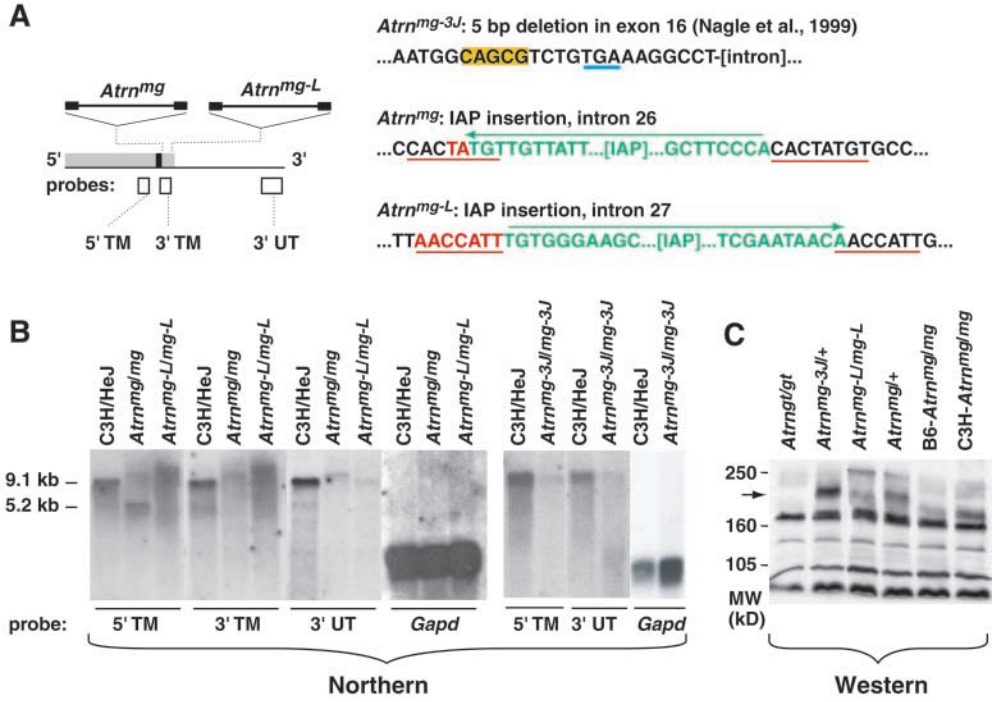

FIGURE 2.—Molecular characterization of *Atrn* mutant alleles. (A) Molecular changes in the *Atrn* locus in $Atrn^{mg\text{-}3J}$, $Atrn^{mg}$, and $Atrn^{mg\text{-}L}$ mutant animals. The mutation in $Atrn^{mg\text{-}3J}$ mice is a 5-bp deletion (boxed in yellow) near the end of exon 16 (NAGLE *et al.* 1999). This deletion causes a frameshift and premature stop three codons downstream (underlined in blue). Both $Atrn^{mg}$ and $Atrn^{mg\text{-}L}$ are caused by IAP insertions in adjacent introns and in opposite orientation. Insertion sites are shown, with IAP sequence in green and orientation of the IAP indicated by a green arrow, novel nucleotides not present in the original *Atrn* intronic sequence or the IAP in red, and repeated sequence flanking and/or overlapping the IAP insertion sites underlined in red. Transcripts that lie upstream of the $Atrn^{mg}$ insertion site are detected by only the 5′ TM probe; transcripts that lie downstream of the $Atrn^{mg}$ insertion site are detected by the 3′ TM probe and the 3′ UTR probe; transcripts that lie upstream of the $Atrn^{mg\text{-}L}$ insertion site are detected by both the 5′ TM probe and the 3′ TM probe; transcripts that lie downstream of the $Atrn^{mg\text{-}L}$ insertion site are detected by both the 3′ TM probe and the 3′ UTR probe (the 3′ TM probe spans the insertion $Atrn^{mg\text{-}L}$ site). (B) Northern hybridization of polyadenylated brain RNA from nonmutant C3H/HeJ and $Atrn^{mg}$, $Atrn^{mg\text{-}L}$, and $Atrn^{mg\text{-}3J}$ homozygotes (2.7 μg of mRNA from $Atrn^{mg\text{-}3J}$ homozygotes and 1.3 μg from the others). The cDNA probes used are described in MATERIALS AND METHODS. $Atrn^{mg}$ and $Atrn^{mg\text{-}L}$ mutants produce reduced levels of normal-sized RNA and also produce RNA fragments of abnormal size; $Atrn^{mg\text{-}3J}$ mutants produce greatly reduced levels of normal-sized RNA that can be detected only in polyadenylated RNA. (C) Western blot analysis of whole brain extracts from *Atrn* mutant mice. The predicted molecular weight of Atrn in the absence of glycosylation is 155 kD; however, endogenous Atrn from brain migrates at ~210 kD (arrow); this protein is absent from $Atrn^{mg\text{-}3J}$ homozygotes (not shown) and from $Atrn^{gt}$ homozygotes. Extracts from $Atrn^{mg\text{-}L}$ homozygous mutants show reduced levels of the ~210-kD protein; extracts from $Atrn^{mg}$ homozygous mutants on either a C3H/HeJ background (C3H-$Atrn^{mg/mg}$) or a C57BL6/J background (B6-$Atrn^{mg/ng}$) show an aberrant protein that migrates slightly faster than endogenous Atrn.

region of the Atrn cDNA (Figure 2B). In addition, a smaller band of ~5.2 kb is detected in $Atrn^{mg}$ but not nonmutant polyadenylated RNA. Analogous to the larger transcript in $Atrn^{mg\text{-}L}$, this likely terminates within the IAP since it is detected only by a cDNA probe (5′ TM, Figure 2A) that lies upstream of the $Atrn^{mg}$ insertion site (Figure 2A). Multiple attempts to isolate the aberrant transcripts in $Atrn^{mg}$ and $Atrn^{mg\text{-}L}$ mice using reverse transcription-PCR and 3′-rapid amplification of cDNA ends (RACE) were unsuccessful (data not shown). Nonetheless, our results indicate that the different effects on splicing in these animals are likely to be a result of opposite orientation of the IAP insertions.

To investigate how the different alleles affected expression of Atrn protein, we examined Western blots of tissue extracts using a polyclonal antisera against residues 666–782 of mouse Atrn. In extracts from whole brain, this antisera detects an ~210-kD protein in nonmutant animals that is not observed in brain extracts from $Atrn^{mg\text{-}3J}$ animals or $Atrn^{gt}$ animals (data not shown and Figure 2C). Extracts from $Atrn^{mg\text{-}L}$ animals show slightly reduced levels of a normal-sized protein, and extracts from $Atrn^{mg}$ animals show an aberrant protein apparently reduced in size by ~20 kD (Figure 2C). These results support the impression based on coat color phenotypes that $Atrn^{mg\text{-}3J}$ is a null or nearly null allele and that $Atrn^{mg\text{-}L}$ is a mild hypomorph.

Effects of *Atrn* alleles on energy balance: As described above, while $Atrn^{mg}$ or $Atrn^{mg\text{-}3J}$ suppress A^y-induced obesity, previous studies have reported conflicting results with regard to the effects of these mutations on body weight in the absence of A^y (MILLER *et al.* 1997; DINULESCU *et al.* 1998; HE *et al.* 2001). In an attempt to resolve these apparent differences, we examined the effects of each *Atrn* allele on body weight in a paradigm that compared littermates in an isogenic or nearly isogenic background. We bred animals homozygous for each of the *Atrn* alleles to nonmutant C3H/HeJ mice and intercrossed or backcrossed their progeny to produce mutant and nonmutant sibs for comparison. We found that male mice homozygous for the $Atrn^{mg}$ and $Atrn^{mg\text{-}3J}$ mutations weighed ~10–15% less than their nonmutant

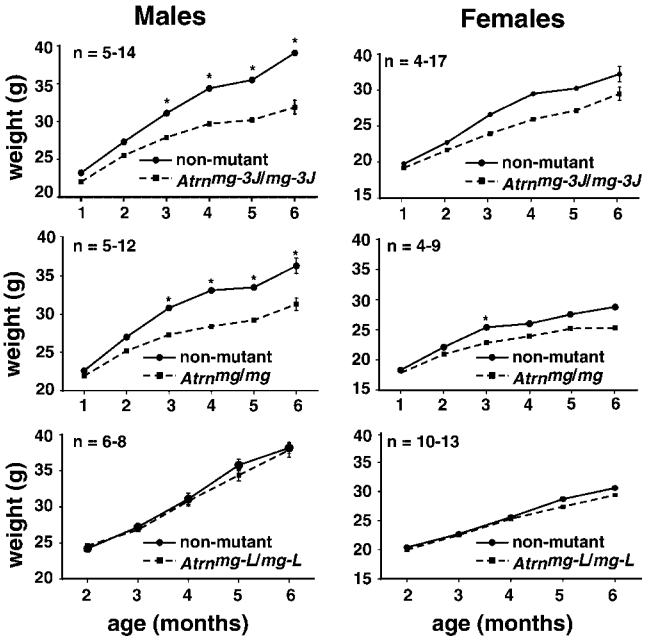

FIGURE 3.—Body weight of mice carrying different *Atrn* alleles. Average weight of male (left) and female (right) *Atrn* mutants and nonmutant littermates is plotted (±SEM) against age. Male $Atrn^{mg\text{-}3J}$ and $Atrn^{mg}$ homozygotes weighed less by 3 months of age, whereas female $Atrn^{mg\text{-}3J}$ and $Atrn^{mg}$ homozygotes showed a trend toward decreased weight at 4 or 3 months of age, respectively. Neither male nor female $Atrn^{mg\text{-}L}$ homozygotes showed evidence of decreased body weight at any of the ages examined. (*, $P < 0.05$).

($Atrn^{+/-}$ or $Atrn^{+/+}$) littermates by 3 months of age (Figure 3). A similar trend was observed in female animals although the differences were significant only ($P < 0.05$) at 3 ($Atrn^{mg}$) and 4 ($Atrn^{mg\text{-}3J}$) months of age (Figure 3). Surprisingly, $Atrn^{mg\text{-}L}$ had no detectable effect on body weight in either males or females up to 6 months of age (Figure 3).

We also evaluated the effects of each allele on adiposity, food consumption, and home cage locomotor activity. For these studies, pairs of mutant and nonmutant littermates at 2–12 months of age were housed individually for 7 days, their food consumption was measured every 24 hr over a 5-day period, their locomotor activity was measured in a photobeam apparatus, and their body fat content was measured by carcass analysis. The $Atrn^{mg}$ and $Atrn^{mg\text{-}3J}$ mutations caused an ~20–40% reduction in body fat content, consistent with the 10–15% reduction in total body weight, whereas the $Atrn^{mg\text{-}L}$ mutation had little or no effect on body fat content (Figure 4). Reduced adiposity could not be accounted for by reduced food intake since none of the three mutations had a significant effect on food consumption (Figure 4), but nocturnal locomotor activity was elevated by 20–30% in $Atrn^{mg\text{-}3J}$ mutants (Figure 5) and by 55–70% in $Atrn^{mg}$ mutants (Figure 5). The $Atrn^{mg\text{-}L}$ mutation had no detectable effect on locomotor activity (Figure 5). With regard to energy balance, these results suggest that the primary defect caused by absence of *Atrn* is increased locomotor activity and consequent energy expenditure and that mutant animals are unable to compensate (by alterations in metabolic rate or food consumption), leading to reduced adiposity and body weight.

During the course of these experiments, we noted a small number of *Atrn* mutant animals that displayed extreme hyperactivity, with a total number of photobeam breaks 5- to 10-fold greater than nonmutant littermates. This phenotype may reflect a distinct pathophysiologic process since it was observed among animals homozygous for each of the *Atrn* alleles, including $Atrn^{mg\text{-}L}$; therefore, animals that displayed extreme hyperactivity were not included in the results shown in Figures 3 and 4. Nonetheless, extreme hyperactivity must be caused by loss of function for Atrn, since the phenotype was observed in 10% of the ~100 mutant animals tested and was never observed in nonmutant littermates.

Effects of *Agouti* on energy balance: The results described above are consistent with a model in which the effects of *Atrn* mutations on body weight regulation are secondary to a more general role in neuronal development. An alternative explanation, however, posits that Atrn plays a specific role in body weight regulation as an accessory receptor for Agouti protein and that *Agouti* itself therefore normally regulates energy balance. While the latter idea is at odds with the view that the effects of *Agouti* are normally limited to pigmentation, it has garnered some support from *in vitro* studies carried out with human adipocytes (XUE *et al.* 1998) and from behavioral studies carried out with deer mice and rats (COTTLE and PRICE 1987; HAYSSEN 1997).

A simple test for the effects on body weight of a wild-type compared to a mutant *Agouti* allele is complicated by the molecular cause of the most common mutant allele, *nonagouti* (*a*), in which an insertion of retrotransposon sequences interferes with, but does not eliminate, normal gene function (BULTMAN *et al.* 1994). However, several point mutations of *Agouti* have been characterized that are amorphic (HUSTAD *et al.* 1995), and one of these, *extreme nonagouti* (a^e), has been bred into a C57BL/6J background, upon which an $A^{w\text{-}J}$ allele is also available.

We crossed C57BL/6J-$A^{w\text{-}J}/A^{w\text{-}J}$ with C57BL/6J-a^e/a^e mice and measured body weight in F_2 littermates. Like $Atrn^{mg\text{-}3J}/Atrn^{mg\text{-}3J}$ mutants, a^e/a^e animals not only make no visible pheomelanin but also have darkly pigmented tails and ears. There was no significant difference in body weight observed between $A^{w\text{-}J}$/- and a^e/a^e male or female mice by 3–4 months of age (Figure 6), a time by which the weight of $Atrn^{mg\text{-}3J}$ and $Atrn^{mg}$ homozygotes does differ from that of their normal sibs (Figure 3). This observation supports the conclusion that the effect of Atrn deficiency on body weight, adiposity, and locomotor activity in $Atrn^{mg\text{-}3J}$ and $Atrn^{mg}$ homozygous mice is due to Agouti-independent action of Attractin.

Effects of *Atrn* alleles on spongy degeneration: The

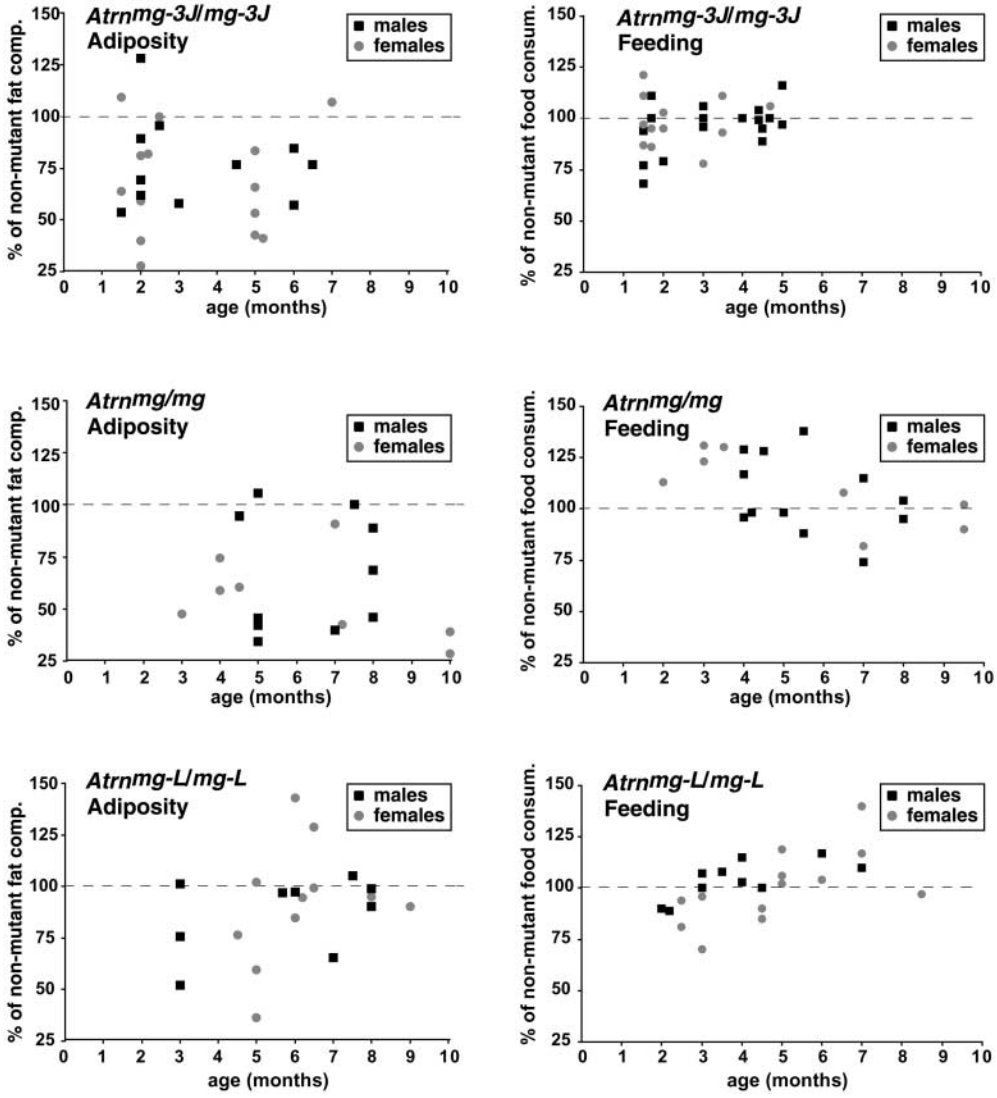

FIGURE 4.—Adiposity (left) and food intake (right) of *Atrn* mutants compared to nonmutant littermates. Body fat composition was determined by carcass analysis as described in MATERIALS AND METHODS; relative fat composition (proportion of body weight accounted for by glycerol) of each mutant animal was calculated as a percentage of the value observed in its nonmutant sib. These percentage values are plotted against age for individual male and female animals homozygous for each of the mutant *Atrn* alleles. Male mice homozygous for each of the three *Atrn* mutations had significantly decreased adiposity; females homozygous for the $Atrn^{mg\text{-}3J}$ or $Atrn^{mg}$ mutation also showed a significant decrease. Considering all ages together, $Atrn^{mg\text{-}3J}$ mutant males ($n = 11$) had an average of 77.4 ± 2.0% (SEM) the fat content of nonmutant sibs ($0.01 > P > 0.001$); $Atrn^{mg\text{-}3J}$ mutant females ($n = 14$), 68.3 ± 1.9% ($P < 0.001$); $Atrn^{mg}$ mutant males ($n = 10$), 66.5 ± 3.0% ($0.01 > P > 0.001$); $Atrn^{mg}$ mutant females ($n = 8$), 55.2 ± 2.5% ($P < 0.001$); $Atrn^{mg\text{-}L}$ mutant males ($n = 9$), 86.9 ± 2.1% ($0.05 > P > 0.02$); and $Atrn^{mg\text{-}L}$ mutant females ($n = 11$), 84.8 ± 3.7% ($0.4 > P > 0.2$). Food intake was measured over five consecutive days to obtain a daily average for *Atrn* mutants and sex-matched littermates. The average daily food consumption of each *Atrn* mutant is given as a percentage of that of its nonmutant sib and plotted against age. The average daily food intake of *Atrn* mutants did not differ significantly from that of their nonmutant sibs (all $P > 0.10$): That of $Atrn^{mg\text{-}3J}$ mutant males was ~93% that of their nonmutant sibs (5.1 *vs.* 5.5 g; $n = 17$); $Atrn^{mg\text{-}3J}$ mutant females, ~98% of nonmutant (4.1 *vs.* 4.2 g; $n = 12$); $Atrn^{mg}$ mutant males, ~104% of nonmutant (5.5 *vs.* 5.2 g; $n = 12$); $Atrn^{mg}$ mutant females, ~108% of nonmutant (5.6 *vs.* 5.2 g; $n = 8$); $Atrn^{mg\text{-}L}$ mutant males, ~104% of nonmutant (5.1 *vs.* 4.9 g; $n = 10$); and $Atrn^{mg\text{-}L}$ mutant females, ~98% of nonmutant (5.1 *vs.* 5.2 g; $n = 13$). If food intake is calculated as a percentage of body weight (average daily weight of food consumed as a percentage of mouse body weight), only $Atrn^{mg}/Atrn^{mg}$ females have a significant ($0.1 > P > 0.05$) increase in food consumption (22.6 *vs.* 18.6% for nonmutant littermates).

widespread CNS distribution of *Atrn* mRNA and the histopathologic abnormalities observed in $Atrn^{mg\text{-}3J}/Atrn^{mg\text{-}3J}$ mice and *zitter* rats suggest that *Atrn* may help to establish and/or maintain normal patterns of neuronal architecture throughout the brain and spinal cord (KONDO *et al.* 1995; HE *et al.* 2001; KURAMOTO *et al.* 2001). Because failure to carry out these functions is a logical cause of the increased locomotor activity we observed in $Atrn^{mg}$ and $Atrn^{mg\text{-}3J}$ mutant mice, we compared the timing and severity of spongy degeneration among mice homozygous for the three different *Atrn* alleles. As with the other phenotypes associated with loss-of-function mutations in *Atrn*, $Atrn^{mg\text{-}3J}$ homozygotes are the most severely affected and $Atrn^{mg\text{-}L}$ homozygotes the least (Figure 7). Vacuoles were found in all regions of the CNS of $Atrn^{mg\text{-}3J}$ mutants by 1 month of age and were exaggerated with increasing age (Table 1). In $Atrn^{mg}$ mutants, vacuoles appeared between 2 and 4 months of age and appeared qualitatively the same as in $Atrn^{mg\text{-}3J}$ mutants, although quantitatively less severe. Vacuoles were not observed in $Atrn^{mg\text{-}L}$ mutants by 4 months of age, but mild vacuolation was apparent in 8-month-old animals, again qualitatively similar to that seen in $Atrn^{mg\text{-}3J}$ and $Atrn^{mg}$ mutants but much less extensive. The later onset and lesser degree of vacuolation in $Atrn^{mg\text{-}L}$ mutants is consistent with our other observations

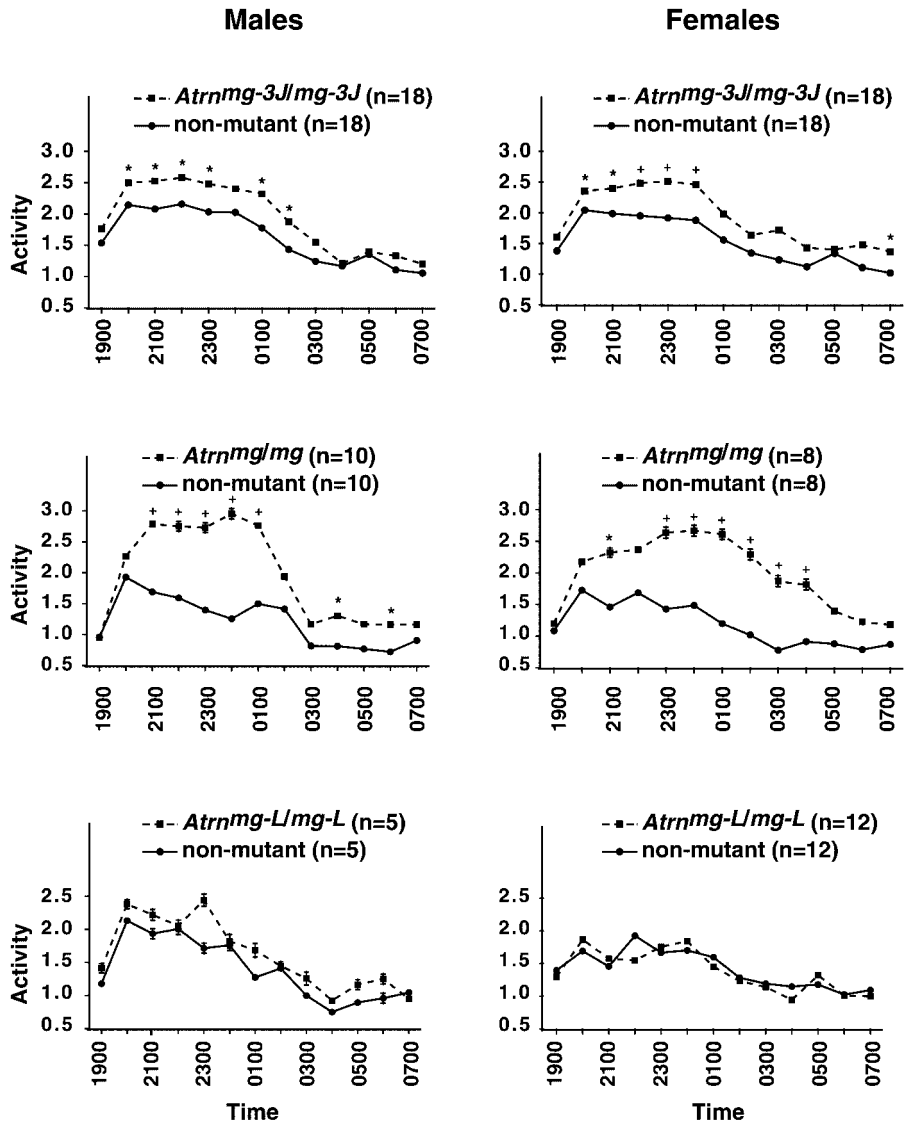

FIGURE 5.—Nocturnal locomotor activity in *Atrn* mutant mice. Activity was measured using a photobeam activity cage system as described in MATERIALS AND METHODS and is given in average number of beam breaks per hour/1000 (±SEM) plotted against time of day for male (left) and female (right) animals. $Atrn^{mg\text{-}3J}$ and $Atrn^{mg}$ homozygotes have significantly increased levels of nocturnal activity relative to their nonmutant littermates, while $Atrn^{mg\text{-}L}$ homozygotes do not (*, $0.05 > P > 0.01$; +, $P < 0.01$).

that this allele has a weaker effect on *Atrn* mutant phenotypes and thus is hypomorphic to $Atrn^{mg}$.

DISCUSSION

The original *mahogany* ($Atrn^{mg}$) mutant was first recognized for its effect on pheomelanogenesis, but subsequent more careful analysis of *Atrn* mutants has led to the identification of additional phenotypes in CNS histology and body weight regulation: Mice homozygous for the $Atrn^{mg\text{-}3J}$ mutation have widespread spongy degeneration of the CNS, show decreased body weight relative to nonmutant sibs, and are resistant to both A^y- and diet-induced obesity (MILLER *et al.* 1997; DINULESCU *et al.* 1998; NAGLE *et al.* 1999; HE *et al.* 2001; KURAMOTO *et al.* 2001). We recently demonstrated that Atrn is a low-affinity receptor for Agouti protein, but additional roles for Atrn that are independent of melanocortin signaling must be responsible for vacuole formation and suppression of diet-induced obesity (HE *et al.* 2001). Here, we find that all three phenotypes—pigmentation, vacuolation, and body weight regulation—are altered in parallel among three *Atrn* alleles with different degrees of severity. These findings furnish insight into the relationship between Atrn structure and function, have implications for *Atrn* as a pharmacologic anti-obesity target, and provide a unifying explanation for the behavioral effects of *Atrn* mutant mice.

Atrn and body weight regulation: $Atrn^{mg\text{-}3J}$ and $Atrn^{mg}$ homozygotes both exhibit a 10–15% reduction in body weight that can be explained by reduced adiposity. These animals exhibit levels of food intake that do not differ from that of their nonmutant siblings and therefore must have increased energy expenditure, probably due to a combination of increased locomotor activity and a muscle tremor (KURAMOTO *et al.* 2001). An alternative explanation—a previously unrecognized role for *Agouti* in energy homeostasis—can be excluded because

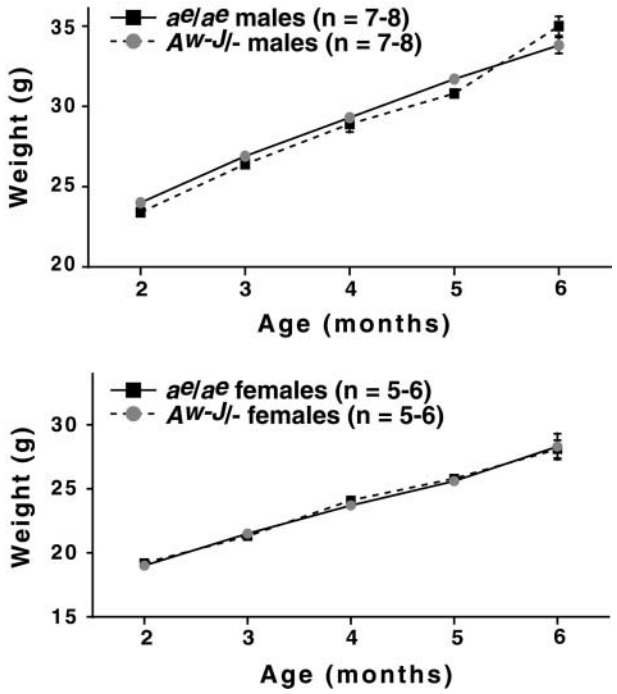

FIGURE 6.—Effect of a loss-of-function *Agouti* allele on weight gain. C57BL/6J animals segregating for $A^{w\text{-}J}$ and a^e alleles at the Agouti locus were weighed monthly and the weight of a^e homozygotes was compared to that of $A^{w\text{-}J}$/- littermates. The mean weights (±SEM) of five to eight mice of each genotype are shown; no significant differences in body weight were detected in animals by 6 months of age.

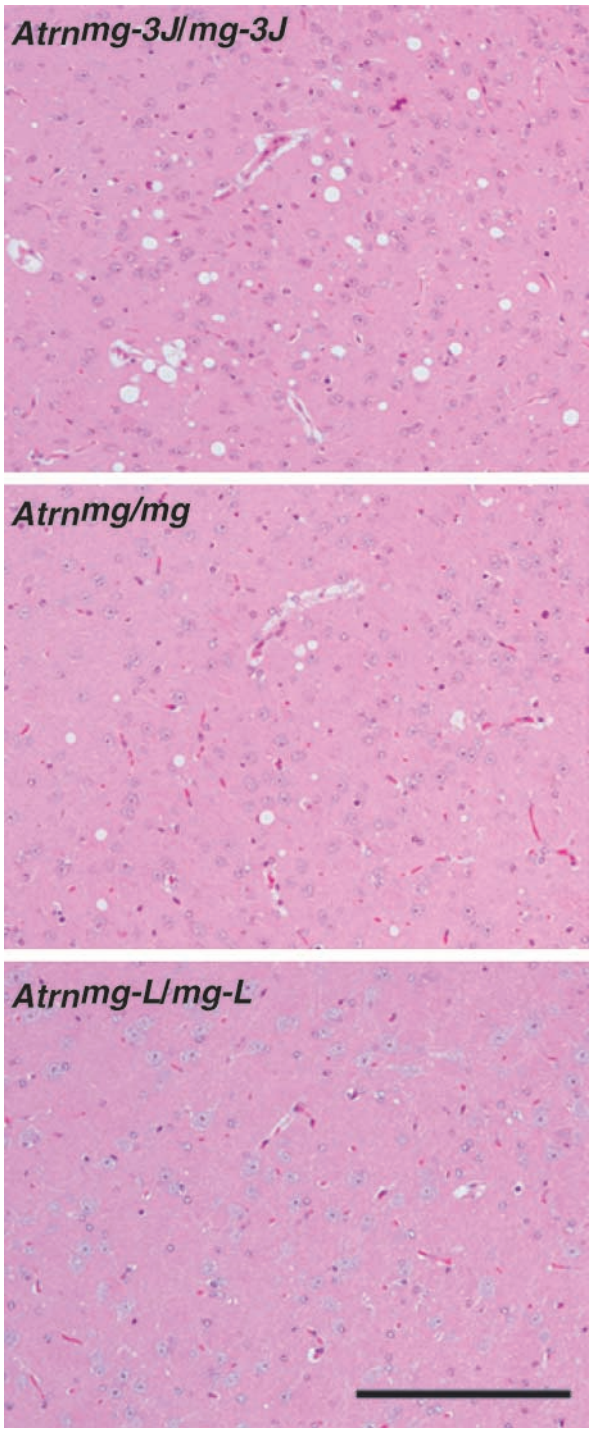

FIGURE 7.—CNS vacuolation in *Atrn* mutants at 4 months of age. All regions of the brain were examined by light microscopy; the results shown are coronal sections through the thalamus, where vacuolation was clear (in $Atrn^{mg\text{-}3J}$ and $Atrn^{mg}$ mutant animals) as compared to other regions. Brain sections from nonmutant animals (not shown) appear identical to $Atrn^{mg\text{-}L}$ animals. Bar, 200 μm.

the weight of animals homozygous for a complete loss-of-function allele of *Agouti*, a^e, is normal.

Increased muscle catabolism or sympathetic activation plays a primary role in other models of body weight dysregulation, *e.g.*, cold exposure (Abelenda and Puerta 1991), uncontrolled diabetes (Williams *et al.* 1989), or overexpression of *Ucp3* in skeletal muscle (Clapham *et al.* 2000), but is usually associated with hyperphagia that partially compensates for the increased energy expenditure. Failure of $Atrn^{mg\text{-}3J}$ and $Atrn^{mg}$ mutant mice to increase their food intake thus represents an additional abnormality caused by loss of function for *Atrn*.

Our observations on food intake and body weight in *Atrn* mutant mice are consistent with those of others (Y. Ogawa, University of Kyoto, unpublished data) who have studied the effect of all three *Atrn* alleles on feeding in a C3H/HeJ background. However, in LDJ/Le $Atrn^{mg}$ mutants crossed into a C57BL/6J background for six to eight generations, Dinulescu *et al.* (1998) reported that mutant animals showed increased food consumption relative to age-matched controls. Possible explanations for this difference include modifier genes or body weight quantitative trait loci closely linked to *Atrn* (Cheverud *et al.* 1996; Lembertas *et al.* 1997) that complicate analysis of the C57BL/6J-$Atrn^{mg}$ animals.

On the basis of the correlation between spongy degeneration and alterations of energy balance in animals carrying the three *Atrn* alleles, we propose that the process responsible for spongy degeneration explains both increased energy expenditure and the failure to compensate appropriately with increased food intake. The

TABLE 1

Progression of spongiform changes in *Atrn* mutants

	Age			
Genotype	1 mo	2 mo	4 mo	8 mo
$Atrn^{mg\text{-}3J}/Atrn^{mg\text{-}3J}$	Moderate	Moderate-severe	Severe	ND
$Atrn^{mg}/Atrn^{mg}$	None	None	Moderate	ND
$Atrn^{mg\text{-}L}/Atrn^{mg\text{-}L}$	None	None	None	Mild

The results shown represent a comparative and qualitative evaluation of vacuoles in the brainstem and cerebral cortex; see Figure 7 for representative examples at 4 months of age. ND, not determined.

central tenet of this hypothesis—that the effects of *Atrn* deficiency on energy homeostasis are caused by structural abnormalities of the CNS—is supported by the lack of behavioral and body weight phenotypes in $Atrn^{mg\text{-}L}$ homozygotes, which have few, if any, abnormalities in brain histology.

This hypothesis could account for the observation of Nagle *et al.* (1999) that $Atrn^{mg\text{-}3J}$ partially suppresses diet-induced obesity, but it is harder to explain why $Atrn^{mg\text{-}3J}$ has no effect on obesity caused by an Agrp transgene (He *et al.* 2001) or why $Atrn^{mg}$ has no effect on obesity caused by the *Mc4r*, *tub*, Cpe^{fat}, or $Lepr^{db}$ mutations (Nagle *et al.* 1999). However, an important characteristic of diet-induced obesity that distinguishes it from obesity caused by defects in leptin or melanocortin signaling is the presence of compensatory hypothalamic responses. In diet-induced obesity, hypothalamic levels of mRNA for Npy and Agrp generally decrease and levels of Pomc usually increase (Levin 1999; Ziotopoulou *et al.* 2000), which can be viewed as an attempt to maintain homeostasis by compensatory hypophagia and increased energy expenditure. By contrast, deficient leptin or melanocortin signaling within the hypothalamus causes hyperphagia and decreased energy expenditure. Thus, in diet-induced obesity, homeostatic mechanisms fail to engage effectors, whereas in obesity caused by defects in leptin or melanocortin signaling, homeostatic mechanisms fail to become engaged.

This conceptual distinction between obesity caused by increased dietary fat and at least some of the monogenic obesities described above might account for the different response to $Atrn^{mg\text{-}3J}$ or $Atrn^{mg}$ as follows. Assuming that defects in leptin or melanocortin signaling have no effect on increased locomotor activity or the tremor caused by *Atrn* mutations, $Lepr^{db}$ or Tg.ActbAgrp animals that are doubly mutant for *Atrn* may be able to "compensate" for their increased energy expenditure by altering food intake and/or autonomic activity. In other words, increased locomotor activity of any source, *e.g.*, due to a mutation or forced exercise, might be a more effective treatment for diet-induced obesity than for hypothalamic obesity. Such a distinction would necessarily be quantitative rather than qualitative, since increased locomotor activity caused by forced exercise or an inner ear defect can reduce but not eliminate obesity caused by leptin deficiency (Mayer 1953).

Overall, the dominance relationships for pigmentation and levels of normal *Atrn* mRNA, with $Atrn^{mg\text{-}3J} < Atrn^{mg} < Atrn^{mg\text{-}L}$, correlate closely with the onset and severity of vacuolation and the nonpigmentary phenotypes. One exception, however, is that the weight, adiposity, and locomotor defects in $Atrn^{mg}$ mutants were approximately equivalent to those in $Atrn^{mg\text{-}3J}$ mutants despite the difference in timing of the appearance of vacuoles in their brains. It is possible that the aberrant protein unique to the $Atrn^{mg}$ allele contributes to behavioral and body weight abnormalities in a neomorphic manner that is independent of vacuolation. It seems more likely, however, that a progressive neurodegenerative process caused by absence of *Atrn* mRNA triggers behavioral abnormalities above a certain threshold, which is exceeded in $Atrn^{mg\text{-}3J}$ and $Atrn^{mg}$ but not in $Atrn^{mg\text{-}L}$ mutant animals. A corollary of this hypothesis is that vacuolation *per se*—at the level of light microscopy—is not the cause of increased energy expenditure but rather an additional consequence of the underlying degenerative process, since increased locomotor activity and reduced adiposity are observed in $Atrn^{mg}$ mutant animals at an age before vacuolation is detectable.

Atrn in the brain: The Atrn protein contains several domains characteristic of molecules involved in axon guidance, and its mRNA is highly expressed during brain development, but neither the *zitter* rat nor *Atrn* mutant mice exhibit gross histological abnormalities until after birth. It is possible that absence of *Atrn* causes subtle defects of neuronal wiring that affect motor function and/or leptin-responsive hypothalamic circuits. Such defects could contribute to increased energy expenditure or the absence of compensatory hyperphagia, respectively, and might be investigated further by tract tracing studies. However, it is important to distinguish axonal guidance abnormalities that occur during development from neurodegenerative changes that occur after birth, since increased locomotor activity and tremor can be caused by many different types of CNS abnormalities (Mayer 1953; Mansuy and Suter 2000).

Although spongiform encephalopathy is perhaps best known as the consequence of transmissible prion-

related diseases, protease sensitivity of Prion protein has been reported to be normal in the *zitter* rat (Gomi *et al.* 1994), and widespread vacuolation can be a nonspecific marker of several different pathophysiologic mechanisms. After birth, *Atrn* mRNA is expressed widely throughout the brain and spinal cord and exhibits cellular specificity without obvious anatomic or functional correlation. For example, *Atrn* mRNA is found in Purkinje cells but not granule cells, in a subset of neurons within certain midbrain nuclei, and in reticular but not pyramidal cells of the hippocampus (Lu *et al.* 1999). The distribution of mRNA corresponds roughly to the distribution of vacuoles; although the level of resolution does not allow any conclusions about cell autonomy of vacuolation, it seems unlikely that the vacuoles are a response to a circulating toxin or metabolite. Furthermore, the levels of vacuolation we observed in $Atrn^{mg\text{-}3J}$, $Atrn^{mg}$, and $Atrn^{mg\text{-}L}$ mutant animals correlate with the levels of normal *Atrn* mRNA, indicating that *Atrn*-induced spongiform degeneration is caused by a loss of function rather than accumulation of abnormal Atrn protein.

Taken together, these considerations suggest that a major function of Atrn is to maintain or stabilize certain classes of cell-cell interactions, and it is an absence of this stabilizing function that causes vacuolation. Extensive neuropathologic studies of *zitter* rats show hypomyelination and synapse degradation with some vacuoles in myelin sheaths, some vacuoles in cell bodies, and occasional postsynaptic dilation of dendrites (Gomi *et al.* 1990; Kondo *et al.* 1991, 1992, 1993, 1995; Kuramoto *et al.* 1998), but the subcellular relationship between vacuoles and Atrn protein has not been determined. Immunolocalization studies of the endogenous protein in combination with *in vitro* assays for neuronal outgrowth and adhesion should provide additional insight into the molecular pathogenesis of neurodegeneration caused by loss of function for *Atrn*.

It is important to note that the questions addressed above—does absence of Atrn cause neurons to develop abnormally, or does absence of Atrn cause neurons to degenerate prematurely?—are not mutually exclusive, and both processes may contribute to increased energy expenditure and the absence of compensatory hyperphagia. In addition, failure to maintain certain classes of cell-cell interactions in the brain or spinal cord is one of a general class of mechanisms proposed to explain the kinetics of neurodegenerative disease by McInnes and colleagues (Clarke *et al.* 2000). According to this "one-hit" hypothesis, mutations that perturb metabolic or cellular homeostasis cause neurodegeneration by increasing susceptibility to stochastic injury, for example, by increasing the likelihood that nuclear aggregates will form from a polyglutamine-containing protein or by random production of reactive oxygen species from an impaired respiratory chain. Neurodegeneration triggered by a stochastic process in *Atrn* mutant mice could explain the relatively large variance in metabolic phenotypes among genetically identical mutant animals as well as the ~5% of *Atrn* mutant animals that displayed extreme hyperactivity.

Atrn and pigmentation: In addition to CNS vacuolation and increased locomotor activity, which are clearly independent of *Agouti* signaling in *Atrn* mutant mice, our analysis of hair melanins points to a subtle effect of *Atrn* on coat color that is also independent of *Agouti*. In addition to the ~10-fold reduction in AHP content caused by suppression of Agouti-induced pheomelanin production, older *Atrn* mutant mice are dark reddish brown, remarkably similar to the wood for which the mutant was originally named, and exhibit a small reduction of the eumelanin derivative PTCA. This mahogany phenotype is visible mainly in older animals and does not show an absolute correlation with reduction of PTCA, as we also observed slight reductions of PTCA in some young animals carrying the $Atrn^{mg\text{-}L}$ allele (our unpublished results). Nonetheless, the dark reddish brown phenotype caused by loss of function for *Atrn* affects the entire hair shaft and is clearly distinct from that caused by loss of function for *Agouti*. Taken together, these observations suggest that *Atrn* has mild effects on pigmentation that are independent of *Agouti* and raise the intriguing possibility that this is the same mechanism by which absence of *Atrn* affects neurons.

Positing a similar role for *Atrn* in neurons and melanocytes could help resolve the puzzle of how a gene found in flies, worms, and mammals came to assume an additional function unique to higher vertebrates (He *et al.* 2001). Melanin polymers composed of aromatic amino acid derivatives are apparent throughout the animal kingdom, but pheomelanin and the Agouti-melanocortin system are found only in vertebrates. An ancestral Atrn protein that served to facilitate or stabilize interactions between neuroectodermal and supporting cells 500 million years ago might well have continued to carry out these roles for neurons and pigment cells in mammals and therefore could easily have been recruited during vertebrate evolution to serve as an accessory receptor for Agouti protein. Thus, loss of the ancestral function for Atrn would account for neurodegeneration and the dark reddish brown color, whereas loss of the more recent function, Agouti binding, would account for suppression of pheomelanin production. According to this hypothesis, one might anticipate finding additional alleles of *Atrn* that interfere with binding to Agouti protein but not with other functions of Atrn and therefore would suppress pheomelanin production but have no effect on neurodegeneration. In addition, careful examination of the skin in older $Atrn^{mg\text{-}3J}$ mutant mice might reveal ultrastructural changes similar to those found in the brain.

Coat color and behavior in laboratory animals: The original mouse *mahogany* mutation has been widely available for 40 years (Lane and Green 1960), and the rat *zitter* mutation was described almost 20 years ago (Rehm

et al. 1982), but no one suspected the same gene was involved until each was isolated separately by positional cloning. This ironic turn of events underscores the relative strengths of different animal models and has implications for mutagenesis screens driven by phenotype. In the case of *mahogany*, the effects on behavior and body weight are sufficiently subtle that a systematic evaluation was required for their detection; in the case of *zitter*, the effects on coat color are readily apparent but only in a pigmented background.

Some large-scale mutagenesis projects are designed to focus on specific phenotypes, while others are based on high-throughput surveys that sample different organ systems. The recent history of *mahogany* and *zitter* emphasizes the utility of both approaches, since detection of nonpigmentary phenotypes in *mahogany* could not have been accomplished without a quantitative assay of behavior, while recognition of the pigmentary phenotype in *zitter* provided a well-established genetic and cell biologic framework with which to understand and study gene action.

Comparison of pigmentary and nonpigmentary phenotypes in *Atrn* mutant mice also highlights the utility of coat color as a tool for studying gene action, since mild hypomorphs like $Atrn^{mg\text{-}L}$ are detectable only by their effects on pigmentation, and manipulating the genetic background can uncover gene dosage effects that would otherwise not be detectable. Identification and analysis of new pigment mutations with phenotypes similar to *mahogany* may provide additional insight into melanocortin signaling and/or the pathogenesis of neurodegeneration. For example, *mahoganoid* is another previously existing mutant that, like *Atrn* mutations, suppresses A^y-induced obesity and lies upstream of *Mc1r* signaling (Miller *et al.* 1997). A simple explanation for these observations postulates that the gene mutated in *mahoganoid* is required for proper expression and/or action of Atrn protein and can be investigated with tools that already exist.

We thank Phil Leighton and Marc Tessier-Lavigne for their generous gift of $Atrn^{g+}/Atrn^{g+}$ mice. We are grateful to Yoshihiro Ogawa for sharing his unpublished data on food consumption in *Atrn* mutant and nonmutant mice, David Kingsley for helpful advice, Xinyun Lu for her insight into the possible roles of Atrn in energy balance, Kira Leuders for information on IAP elements, and Jean Westerman and Linda Siracusa for C3H/HeJ-$Atrn^{mg\text{-}L}/Atrn^{mg\text{-}L}$ and C57BL/6J-a^{y}/a^{y} mice, respectively. We also thank Phil Kim for technical assistance, Jason Mastaitis and Terry Flier for advice regarding saponification, and Andrzej Chruscinski for instruction on the photobeam cage system. This work was supported by a National Institutes of Health grant to G.S.B. (DK-48506) and by an American Heart Association Western States fellowship award to T.M.G. G.S.B. is an Associate Investigator of the Howard Hughes Medical Institute.

LITERATURE CITED

Abelenda, M., and M. L. Puerta, 1991 Relationship among food intake, thyroid status and chronic cold-exposure in the rat. Horm. Metab. Res. **23:** 90–91.

Bultman, S. J., M. L. Klebig, E. J. Michaud, H. O. Sweet, M. T. Davisson *et al.*, 1994 Molecular analysis of reverse mutations from nonagouti (A) to Black-and-Tan (A(T)) and White-Bellied agouti (A(W)) reveals alternative forms of agouti transcripts. Genes Dev. **8:** 481–490.

Cheverud, J. M., E. J. Routman, F. A. Duarte, B. van Swinderen, K. Cothran *et al.*, 1996 Quantitative trait loci for murine growth. Genetics **142:** 1305–1319.

Clapham, J. C., J. R. Arch, H. Chapman, A. Haynes, C. Lister *et al.*, 2000 Mice overexpressing human uncoupling protein-3 in skeletal muscle are hyperphagic and lean. Nature **406:** 415–418.

Clarke, G., R. A. Collins, B. R. Leavitt, D. F. Andrews, M. R. Hayden *et al.*, 2000 A one-hit model of cell death in inherited neuronal degenerations. Nature **406:** 195–199.

Cottle, C. A., and E. O. Price, 1987 Effects of the nonagouti pelage-color allele on the behavior of captive wild Norway rats (Rattus norvegicus). J. Comp. Psychol. **101:** 390–394.

Dinulescu, D. M., W. Fan, B. A. Boston, K. McCall, M. L. Lamoreux *et al.*, 1998 Mahogany (mg) stimulates feeding and increases basal metabolic rate independent of its suppression of agouti. Proc. Natl. Acad. Sci. USA **95:** 12707–12712.

Festing, M. F. W., 1996 Origins and characteristics of inbred strains of mice, pp. 1537–1576 in *Genetic Variants and Strains of the Laboratory Mouse*, edited by M. Lyon, S. Rastan and S. D. M. Brown. Oxford University Press, Oxford.

Gomi, H., K. Inui, H. Taniguchi, Y. Yoshikawa and K. Yamanouchi, 1990 Edematous changes in the central nervous system of zitter rats with genetic spongiform encephalopathy. J. Neuropathol. Exp. Neurol. **49:** 250–259.

Gomi, H., T. Ikeda, T. Kunieda, S. Itohara, S. B. Prusiner *et al.*, 1994 Prion protein (PrP) is not involved in the pathogenesis of spongiform encephalopathy in zitter rats. Neurosci. Lett. **166:** 171–174.

Gunn, T. M., K. A. Miller, L. He, R. W. Hyman, R. W. Davis *et al.*, 1999 The mouse mahogany locus encodes a transmembrane form of human attractin. Nature **398:** 152–156.

Hayssen, V., 1997 Effects of the nonagouti coat-color allele on behavior of deer mice (Peromyscus maniculatus): a comparison with Norway rats (Rattus norvegicus). J. Comp. Psychol. **111:** 419–423.

He, L., T. M. Gunn, D. M. Bouley, X. Y. Lu, S. J. Watson *et al.*, 2001 A biochemical function for attractin in agouti-induced pigmentation and obesity. Nat. Genet. **27:** 40–47.

Hein, L., G. S. Barsh, R. E. Pratt, V. J. Dzau and B. K. Kobilka, 1995 Behavioural and cardiovascular effects of disrupting the angiotensin II type-2 receptor in mice. Nature **377:** 744–747.

Hustad, C. M., W. L. Perry, L. D. Siracusa, C. Rasberry, L. Cobb *et al.*, 1995 Molecular genetic characterization of six recessive viable alleles of the mouse agouti locus. Genetics **140:** 255–265.

Huszar, D., C. A. Lynch, V. Fairchild-Huntress, J. H. Dunmore, Q. Fang *et al.*, 1997 Targeted disruption of the melanocortin-4 receptor results in obesity in mice. Cell **88:** 131–141.

Inui, T., T. Yamamura, H. Yuasa, Y. Kawai, A. Okaniwa *et al.*, 1990 The spontaneously epileptic rat (SER), a zitter*tremor double mutant rat: histopathological findings in the central nervous system. Brain Res. **517:** 123–133.

Ito, S., and K. Fujita, 1985 Microanalysis of eumelanin and pheomelanin in hair and melanomas by chemical degradation and liquid chromatography. Anal. Biochem. **144:** 527–536.

Ito, S., and K. Wakamatsu, 1998 Chemical degradation of melanins: application to identification of dopamine-melanin. Pigment Cell Res. **11:** 120–126.

Jackson, I. J., 1994 Molecular and developmental genetics of mouse coat color. Annu. Rev. Genet. **28:** 189–217.

Kondo, A., Y. Sato and H. Nagara, 1991 An ultrastructural study of oligodendrocytes in zitter rat: a new animal model for hypomyelination in the CNS. J. Neurocytol. **20:** 929–939.

Kondo, A., S. Sendoh, K. Akazawa, Y. Sato and H. Nagara, 1992 Early myelination in zitter rat: morphological, immunocytochemical and morphometric studies. Brain Res. Dev. Brain Res. **67:** 217–228.

Kondo, A., S. Sendoh, J. Takamatsu and H. Nagara, 1993 The zitter rat: membranous abnormality in the Schwann cells of myelinated nerve fibers. Brain Res. **613:** 173–179.

Kondo, A., S. Sendoh, K. Miyata and J. Takamatsu, 1995 Spongy

degeneration in the zitter rat: ultrastructural and immunohistochemical studies. J. Neurocytol. **24:** 533–544.

Kuramoto, T., K. Yamasaki, A. Kondo, K. Nakajima, M. Yamada *et al.*, 1998 Production of WTC.ZI-zi rat congenic strain and its pathological and genetic analyses. Exp. Anim. **47:** 75–81.

Kuramoto, T., K. Kitada, T. Inui, Y. Sasaki, K. Ito *et al.*, 2001 Attractin/Mahogany/Zitter plays a critical role in myelination of the central nervous system. Proc. Natl. Acad. Sci. USA **98:** 559–564.

Lane, P. W., and M. C. Green, 1960 Mahogany, a recessive color mutation in linkage group V of the mouse. J. Hered. **51:** 228–230.

Leighton, P. A., K. J. Mitchell, L. V. Goodrich, X. Lu, K. Pinson *et al.*, 2001 Defining brain wiring patterns and mechanisms through gene trapping in mice. Nature **410:** 174–179.

Lembertas, A. V., L. Perusse, Y. C. Chagnon, J. S. Fisler, C. H. Warden *et al.*, 1997 Identification of an obesity quantitative trait locus on mouse chromosome 2 and evidence of linkage to body fat and insulin on the human homologous region 20q. J. Clin. Invest. **100:** 1240–1247.

Levin, B. E., 1999 Arcuate NPY neurons and energy homeostasis in diet-induced obese and resistant rats. Am. J. Physiol. **276:** R382–387.

Lowell, B. B., V. S-Susulic, A. Hamann, J. A. Lawitts, J. Himms-Hagen *et al.*, 1993 Development of obesity in transgenic mice after genetic ablation of brown adipose tissue. Nature **366:** 740–742.

Lu, X., T. M. Gunn, K. Shieh, G. S. Barsh, H. Akil *et al.*, 1999 Distribution of Mahogany/Attractin mRNA in the rat central nervous system. FEBS Lett. **462:** 101–107.

Mansuy, I. M., and U. Suter, 2000 Mouse genetics in cell biology. Exp. Physiol. **85:** 661–679.

Mayer, J., 1953 Decreased activity and energy balance in the hereditary obesity-diabetes syndrome of mice. Science **117:** 504–505.

Miller, K. A., T. M. Gunn, M. M. Carrasquillo, M. L. Lamoreux, D. B. Galbraith *et al.*, 1997 Genetic studies of the mouse mutations mahogany and mahoganoid. Genetics **146:** 1407–1415.

Nagle, D. L., S. H. McGrail, J. Vitale, E. A. Woolf, B. J. Dussault, Jr. *et al.*, 1999 The mahogany protein is a receptor involved in suppression of obesity. Nature **398:** 148–152.

Ollmann, M. M., B. D. Wilson, Y. K. Yang, J. A. Kerns, Y. Chen *et al.*, 1997 Antagonism of central melanocortin receptors in vitro and in vivo by agouti-related protein. Science **278:** 135–138.

Ozeki, H., S. Ito, K. Wakamatsu and T. Hirobe, 1995 Chemical characterization of hair melanins in various coat-color mutants of mice. J. Invest. Dermatol. **105:** 361–366.

Rehm, S., P. Mehraein, A. P. Anzil and F. Deerberg, 1982 A new rat mutant with defective overhairs and spongy degeneration of the central nervous system: clinical and pathologic studies. Lab. Anim. Sci. **32:** 70–73.

Shimada, M., N. A. Tritos, B. B. Lowell, J. S. Flier and E. Maratos-Flier, 1998 Mice lacking melanin-concentrating hormone are hypophagic and lean. Nature **396:** 670–674.

Shutter, J. R., M. Graham, A. C. Kinsey, S. Scully, R. Luthy *et al.*, 1997 Hypothalamic expression of ART, a novel gene related to agouti, is up-regulated in obese and diabetic mutant mice. Genes Dev. **11:** 593–602.

Williams, G., J. S. Gill, Y. C. Lee, H. M. Cardoso, B. E. Okpere *et al.*, 1989 Increased neuropeptide Y concentrations in specific hypothalamic regions of streptozocin-induced diabetic rats. Diabetes **38:** 321–327.

Xue, B., N. Moustaid-moussa, W. O. Wilkison and M. B. Zemel, 1998 The agouti gene product inhibits lipolysis in human adipocytes via a Ca2+-dependent mechanism. FASEB J. **12:** 1391–1396.

Yang, Y. K., D. A. Thompson, C. J. Dickinson, J. Wilken, G. S. Barsh *et al.*, 1999 Characterization of Agouti-related protein binding to melanocortin receptors. Mol. Endocrinol. **13:** 148–155.

Ziotopoulou, M., C. S. Mantzoros, S. M. Hileman and J. S. Flier, 2000 Differential expression of hypothalamic neuropeptides in the early phase of diet-induced obesity in mice. Am. J. Physiol. Endocrinol. Metab. **279:** E838–845.

Communicating editor: N. A. Jenkins